# Electrostatic properties of C-S-H and C-A-S-H for predicting calcium and chloride adsorption

Satoshi Yoshida [1], Yogarajah Elakneswaran [1,*], Toyoharu Nawa [2]

[1] Division of Sustainable Resources Engineering
Faculty of Engineering, Hokkaido University
Kita 13, Nishi 8, Kita-ku, Sapporo, 060-8628, Japan

[2] Hokkaido University
Kita 8, Nishi 5, Kita-ku, Sapporo, 060-0808, Japan

* Corresponding author
E-mail: elakneswaran@eng.hokudai.ac.jp
Tel: +81-11-706-7274

**Abstract**

The adsorption capacity of cement hydrates considerably affects the ionic ingress into cementitious materials. In this study, the surface electrostatic properties of calcium silicate hydrate (C-S-H) and calcium aluminosilicate hydrate (C-A-S-H) were determined to understand the effects of the properties on calcium and chloride adsorption. The density of the surface functional groups was determined by analysing the structure of C-S-H and C-A-S-H through $^{27}$Al and $^{29}$Si MAS NMR. The surface sites of ≡SiOH and ≡AlOH are available in C-A-S-H whereas C-S-H has ≡SiOH groups for ionic adsorption. We found that the incorporation of aluminium decreases the number of total adsorption sites in C-A-S-H. Furthermore, the site density increased with Ca/(Si+Al). To understand the C-A-S-H/solution interface, a triple-layer surface complexation model was

developed and the associated equilibrium constants for deprotonation, calcium, and chloride adsorption were determined by fitting the experimental data of potentiometric titration and zeta potential measurement results. The estimated surface complexation modelling parameters were verified by predicting the experimental data of calcium and chloride adsorption on C-S-H and C-A-S-H.

**Keywords:** Adsorption; Calcium-Silicate-Hydrate (C-S-H); Chloride; Zeta potential; Surface Complexation model

## 1. Introduction

The characteristics of the cement paste matrix and concrete—such as porosity, tortuosity, the composition of cement hydrates, and the properties of calcium silicate hydrate (C-S-H), which is the main component of hydrated cement—significantly influence the uptake of chloride from the external source and transport it to a greater depth via diffusion [1-4]. The penetrated chloride partially reacts with monosulfoaluminate ($Ca_4Al_2(SO_4)(OH)_{12}\cdot 6H_2O$) and forms Friedel's salt ($Ca_4Al_2Cl_2(OH)_{12}\cdot 4H_2O$). Another part of chloride may be adsorbed on the surface of C-S-H through electrostatic interaction called physical adsorption, and the remaining chloride remains in the pore solution as free chloride, contributing to the initiation of corrosion in reinforcement. Therefore, the sorption ability of cement hydrates significantly influences the concentration of free chloride in the pore solution [5-8]. It has been reported that a partial replacement of ordinary Portland cement (OPC) by supplementary cementitious materials (SCMs), such as fly ash, ground granulated blast-furnace slag, and calcinated clay, not only increases chloride binding, but also shows high resistance to chloride ingress by densifying the microstructure [9-10]. Furthermore, the physical adsorption of chloride is more dominant than the formation of Friedel's salt in SCM [3, 5, 11, 12].

Numerous experimental and modelling studies have reported the interaction of chloride with cement hydrates [2-8, 10-16]. It is widely accepted that the formation of Friedel's salt occurs through the thermodynamic equilibrium between chloride and monosulfoaluminate, called the chemical binding of chloride. However, the physical adsorption of chloride is still subject to debate. Hirao et al. proposed Langmuir chloride adsorption through adsorption experiments [6]. Beaudoin et al. showed that the $H_2O$-$SiO_2$ and $CaO$-$SiO_2$ ratios of C-S-H significantly affect the chloride adsorption on its surface [5]. De Weerdt's group studied a lot of experimental and thermodynamic modelling of chloride binding and analysed the effect of associated cations on the chloride adsorption on the C-S-H surface [14]. They concluded that more adsorption was observed when associated cations of calcium or magnesium were used compared with sodium, and the adsorbed chloride is in the diffuse layer of C-S-H, which is available for diffusion [14]. A significant amount of temperature-dependent chloride adsorption has been reported for fly ash-blended cement paste [12]. Elakneswaran et al. highlighted that the chloride adsorption on C-S-H occurs via calcium-adsorbed surface sites and proposed a double layer surface complexation model to predict chloride adsorption in hydrated OPC [8, 10]. In addition, the model is coupled with a reactive transport equation to simulate chloride ingress [3]. On the other hand, it has been reported that there is no specific adsorption of chloride on C-S-H, and it accumulates on the diffuse layer [15]. Therefore, the proposed hypotheses and experimental results on chloride adsorption on C-S-H are inconsistent and contradictory; more detailed experimental and modelling studies are necessary to understand chloride interactions with C-S-H.

Alumina-rich SCMs increase the incorporation of aluminium in C-S-H and form calcium aluminosilicate hydrate (C-A-S-H) phase [17-21]. The surface chemistry of C-A-S-H is significantly different from that of conventional C-S-H and thus has an impact on the ionic adsorption behaviour. Only a few studies have been conducted on the ionic adsorption on the C-A-S-H surface [21-24]. To the best of our knowledge, there is no comprehensive study on chloride

interaction towards C-A-S-H. C-S-H possesses the surface functional group of the silanol site (≡SiOH). At high pH, the ≡SiOH group deprotonates to $\equiv SiO^-$ and calcium can compensate for the negative surface and change to a positive surface at high calcium concentrations. The partial substitution of Si by Al in the silica tetrahedra could induce forming ≡AlOH surface functional groups in C-A-S-H, in addition to ≡SiOH, and this would influence C-A-S-H surface characteristics. Therefore, more studies on the surface electrical properties of C-A-S-H phase (described by the types of surface functional groups and their densities) are necessary to describe the ionic adsorption behaviour in SCM.

The main purpose of this study is to analyse the interface between C-S-H/C-A-S-H phase and the solution to understand its surface characteristics for calcium and chloride adsorption. The synthesised C-S-H and C-A-S-H were characterised by solid-phase analysis to determine the surface functional groups. Potentiometric titration, zeta potential, and adsorption experiments were carried out to propose and validate a triple-layer surface complexation model for C-S-H/ and C-A-S-H/solution interface.

## 2. Materials and methods

### 2.1 Synthesis of C-S-H and C-A-S-H

In this study, both C-S-H and C-A-S-H were synthesised at 50 °C. The $Ca(OH)_2$ (special grade reagent manufactured by Kanto Chemical Co.) and $SiO_2$ (AEROSIL200 with purity of 99.9% or higher by Nippon Aerosil Co., Ltd.) in different proportions were mixed with pure water with a water to powder ratio of 20 mL/g, and the mixture was cured for 10 days. The targets of the Ca/Si ratios were 0.8, 1.0, and 1.5. In the preparation of C-A-S-H, $Ca(OH)_2$, $SiO_2$, and $CaAl_2O_4$ were mixed for the target of Ca/(Si+Al) of 0.8, 1.0, and 1.5, and Al/Si of 0.19. The mix proportions are reported in **Table 1**. The mixing water to powder ratio was 45 mL/g, and the mixture was sealed after $N_2$ purging and cured for 5 weeks at 50 °C. After the curing time, the solid and liquid phases

were separated by suction filtration, and the solid phase was washed with deionised water three times and then dried for 2 days by freeze-drying before use.

**Table 1:** Mixing proportions for C-S-H and C-A-S-H preparation

| Sample ID | Target Ca/(Si+Al) | Target Al/Si | Initial CaO (mol) | Initial $SiO_2$ (mol) | Initial $CaOAl_2O_3$ (mol) |
|---|---|---|---|---|---|
| CSH-0.8 | 0.80 | - | 0.80 | 1.00 | - |
| CSH-1.0 | 1.00 | - | 1.00 | 1.00 | - |
| CSH-1.5 | 1.50 | - | 1.50 | 1.00 | - |
| CASH-0.8 | 0.80 | 0.19 | 0.72 | 0.84 | 0.08 |
| CASH-1.0 | 1.00 | 0.19 | 0.92 | 0.84 | 0.08 |
| CASH-1.5 | 1.50 | 0.19 | 1.42 | 0.84 | 0.08 |

## 2.2 Experimental procedure

C-S-H and C-A-S-H were characterised by a Rigaku X-ray generator with CuKa radiation, and the measurement conditions were tube voltage 40 kV, scanning range of 5 to 70 ° (2θ), sampling width of 0.02 ° (2θ), and scan speed of 6.5 ° / min. A fluorescent X-ray analyser element monitor EA1200VX manufactured by Hitachi High-Tech Science was used to determine the solid composition of C-S-H and C-A-S-H. The measurement conditions were target Rh, an excitation voltage of 15 kV, and no primary filter. The measurements were conducted in a vacuum atmosphere. Thermogravimetry/Differential Thermal Analysis (TG/DTA) was performed in nitrogen using a HITACHI TG/DTA 7220 analyser at a heating rate of 293 K/min up to 980 °C. The specific surface areas of C-S-H and C-A-S-H were measured using the Brunauer−Emmett−Teller (BET) water adsorption method. Before the measurement, each sample was vacuum-degassed and dried for one hour. Titration experiments for C-S-H and C-A-S-H suspensions were conducted using an automated titration system. A 0.01 mol/L $NaNO_3$ solution (50 mL) was prepared, and the

pH of the solution with 5g/L of C-S-H/C-A-S-H and without C-S-H/C-A-S-H was measured by titrating the solution with 0.25 mol/L NaOH. The suspension was equilibrated for one day and was stirred for three minutes using an ultrasonic cleaner before titration. The $^{29}Si$ MAS NMR experiment was conducted on MSL 400 9.4 T BRUKER at 79.48 MHz. The $Q_8M_8$ (Si $(CH_3)_8Si_8O_2$) manufactured by Wako Pure Chemical Industries was used as a reference material for the measurement. The measurement conditions for each sample were 90 ° pulse length of 5 μs for $^{29}Si$ recycling delay of 45 s and 2000 scans and 4 kHz of the number of rotations. The Win-nut program was used for the analysis of $^{29}Si$ MAS NMR data. A JEOL ECA-700 was used to obtain $^{27}Al$ spectra, where $AlCl_3 \bullet 6H_2O$ was used as a reference material. The measurement conditions for the $^{27}Al$ spectra were 90 ° pulse length of 2.09 μs, delay time of 30 s, 2880 scans, and 18 kHz of spinning rates with 3.2 mm MAS probe. The number of scans for CASH-1.5 was set to 5760 times, as it was considered to have a small amount of Al uptake. All spectra were deconvoluted using the Delta program.

A C-S-H/C-A-S-H suspension with a solid to liquid ratio of 0.1 g/L was prepared for zeta potential measurement using a Zetasizer Nano series. The equilibrium time for the suspension in $Ca(OH)_2$ solution was one day, whereas two days were adopted for the $CaCl_2$ solution. The ionic strength of the solution was adjusted by $NaNO_3$ and kept constant at 20 mmol/L. The suspension was stirred for 3 min using an ultrasonic cleaner before measurement at 25 °C. The average of five measurements was used as the zeta potential value. A batch experiment was performed with $Ca(OH)_2$ solution to determine calcium adsorption on C-S-H/C-A-S-H. The sample was immersed in different concentrations of 10 mL $Ca(OH)_2$ solution for one day, where 5 g/L of solid to liquid ratio was adopted. After equilibrium, the solid and liquid phases were separated by handshaking, and then the liquid phase was filtered with a 0.45 μm syringe filter. The concentration of calcium in the filtered solution was measured by ICP-OES. The calcium concentration difference between the blank and C-S-H/C-A-S-H suspensions was the adsorbed calcium. In addition, the measured

calcium concentration for the C-S-H/C-A-S-H suspension in water was considered as the dissolved calcium from the sample, which was considered in by calculating the amount of adsorbed calcium. The same experimental procedure was adopted for chloride adsorption. C-S-H/C-A-S-H was equilibrated with different concentrations of 5 mL $CaCl_2$ for 5 days, and the solid to liquid ratio for the chloride adsorption was 100 g/L. After equilibrium, the solid and liquid phases were separated and the chloride concentration in the liquid phase was measured using ion chromatography to determine its adsorption.

### 2.3 Modelling approach

The geochemical code PHREEQC was used for the speciation, thermodynamic equilibrium, and surface complexation modelling calculations [25-26]. The charge-distribution-multi site complexation model (CD-MUSIC) available in PHREEQC was adopted for the surface complexation reaction between C-S-H/C-A-S-H and ionic species [27-28], as illustrated in **Fig. 1**. The surface has three planes: the 0-, 1-, and 2-planes. The surface groups of C-S-H/C-A-S-H are located at the 0-plane, and the diffuse layer begins at the 2-plane. The potential at the 0-plane is the surface potential, and the zeta potential can be directly compared with the potential at the 2-plane. The CD-MUSIC model requires the capacitance of the layers and change in charge at three layers because of the dissociation of surface sites and adsorption of ions on the sites, in addition to surface site density and equilibrium constants. The model can be implemented in PHREEQC using the keyword data block of SURFACE and SURFACE_SPECIES with the charge distribution and the capacitance of the inner and outer Stern layers [22].

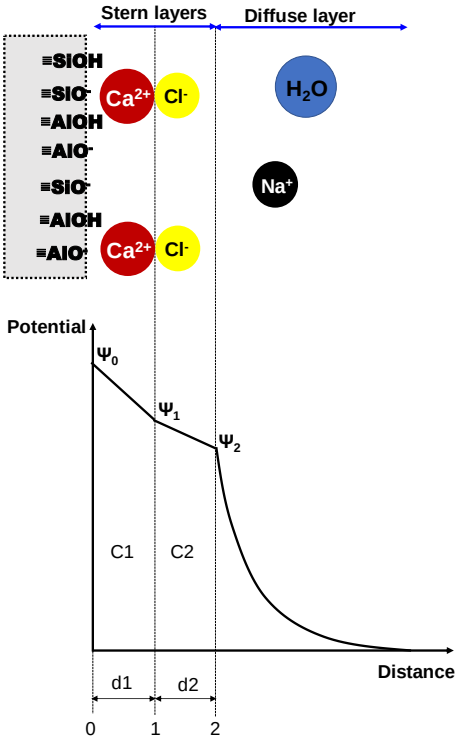


**Fig. 1.** Schematic of the electrical triple-layer used in the CD-MUSIC model.

## 3. Results and discussion

### 3.1 Characterisation and determination of surface site density of C-S-H and C-A-S-H

To calculate the ionic adsorption using a surface complexation model, the types of surface functional groups and their densities must be evaluated. The synthesised C-S-H/C-A-S-H samples were characterised, and this information was used to evaluate the surface site densities. The XRD patterns of the synthesised samples are aligned with the results reported by Myer et al. [29], which was again confirmed by the TG/DTA (refer **Appendix A**). In addition, XRF measurements were conducted on the synthesised samples to examine if the actual Ca/(Si+Al) ratio reaches the target value (**Table 2**). In the samples with Ca/(Si+Al) of 0.8 and 1.0, the measured ratio was almost the same as the target value. However, in the sample with a Ca/(Si+Al) of 1.5, the measured ratio was lower than the target value. It is believed that a part of calcium in the samples was dissolved by washing with de-ionic water in the preparation of the samples. Moreover, the higher water to solid ratio (w/s = 45) adopted in the experiments provides high concentration of calcium in the solution, which reduces the calcium in the samples. $^{29}$Si and $^{27}$Al NMR were used to characterise C-S-H and

C-A-S-H (refer **Appendix A**). The calculated mean chain length (MCL) of the samples, as a function of Ca/(Si+Al), is shown in **Fig. 2.** It is confirmed that MCL decreases with an increase in the Ca/(Si+Al) ratio due to a decrease in the $Q^2b$ proportion. Furthermore, the substitution of Si by Al increases the MCL.

**Table 2:** XRF results on C-S-H and C-A-S-H

| Sample ID | Target Ca/(Si+Al) | Measured Ca/(Si+Al) | Target Al/Si | Measured Al/Si |
|---|---|---|---|---|
| CSH-0.8 | 0.80 | 0.86 | - | - |
| CSH-1.0 | 1.00 | 1.01 | - | - |
| CSH-1.5 | 1.50 | 1.34 | - | - |
| CASH-0.8 | 0.80 | 0.94 | 0.19 | 0.11 |
| CASH-1.0 | 1.00 | 1.08 | 0.19 | 0.13 |
| CASH-1.5 | 1.50 | 1.37 | 0.19 | 0.13 |

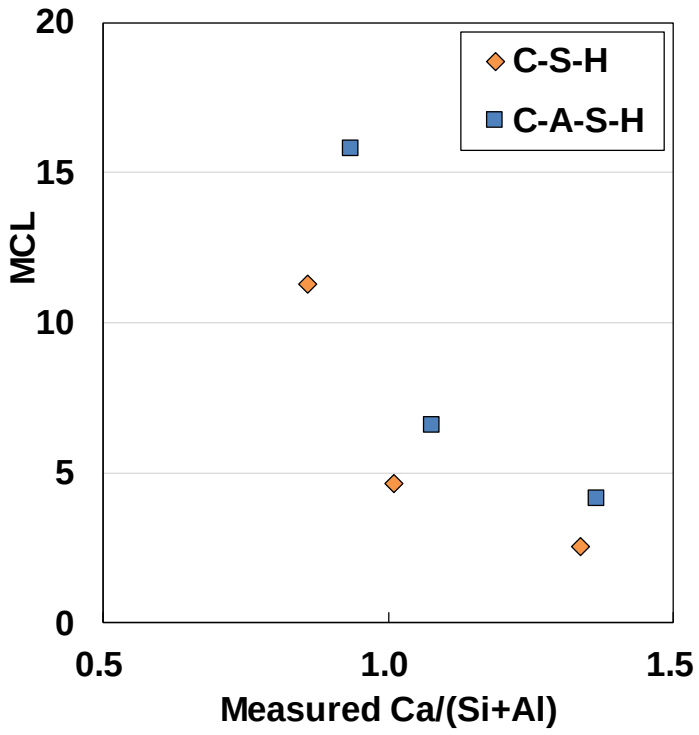

**Fig. 2.** Mean chain length of synthesised C-S-H and C-A-S-H.

The calculated specific surface from the water vapor adsorption data using BET method is shown in **Fig. 3.** as a function of Ca/(Si+Al) ratio. The Ca/(Si+Al) and aluminium incorporation affect the specific surface area, which increases with decreasing Ca/(Si+Al) and aluminium substitution. Haas et al. (2015) reported that there is a correlation between Ca/(Si+Al) and the number of layers in α, β, and γ-C-S-H [30]. Therefore, in this study, it was assumed that the synthesised C-S-H corresponded to β-C-S-H, and the layers were calculated from the results of the specific surface area. The results are shown in **Fig. 4**, as a function of the Ca/(Si+Al) ratio, and it increases with an increase in Ca/(Si+Al).

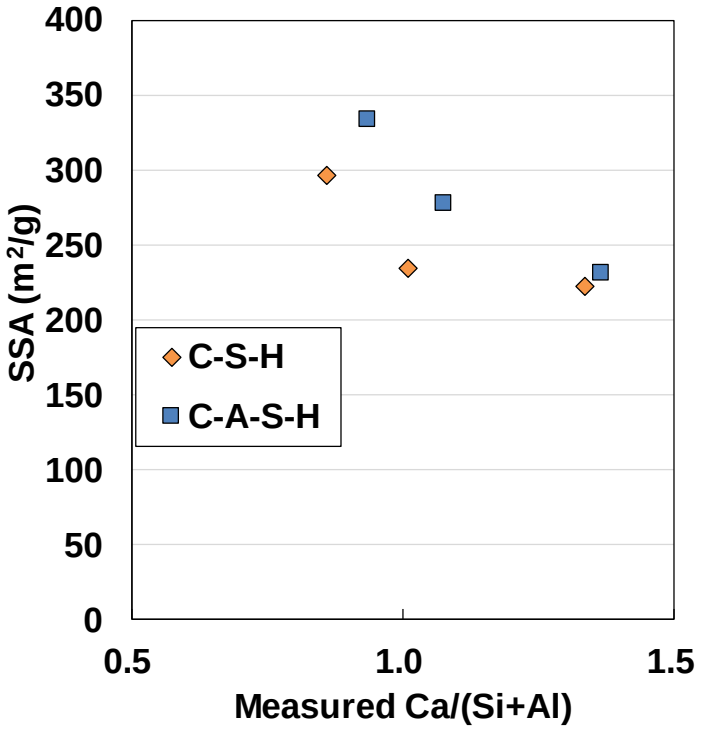


**Fig. 3.** Specific surface area of synthesised C-S-H and C-A-S-H.

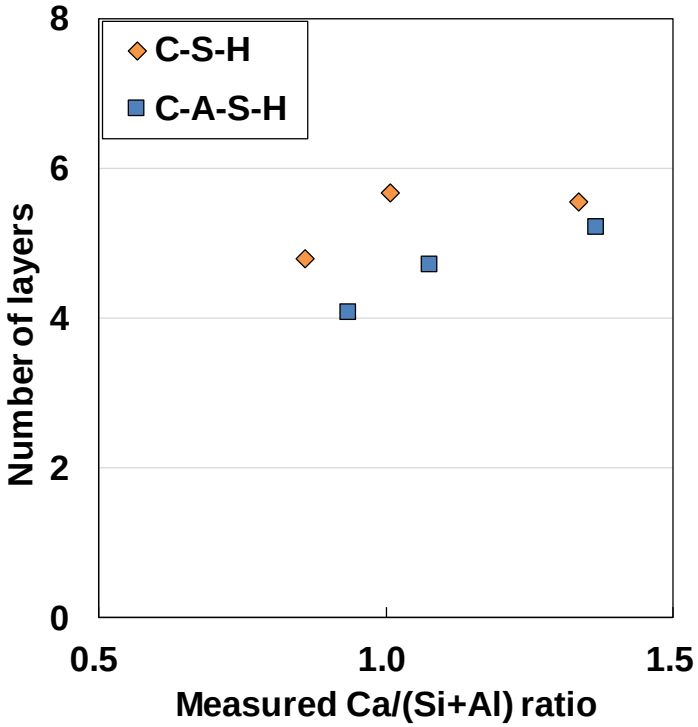


**Fig. 4.** The number of staking layers in synthesised C-S-H and C-A-S-H.

Information about the number of layers was used to estimate the surface site density of C-S-H and C-A-S-H. It was assumed that the structure of C-S-H and C-A-S-H is close to tobermorite-type crystal structure [19], and the C-S-H has surface functional group of ≡SiOH, whereas C-A-S-H possesses both ≡SiOH and ≡AlOH groups. The basic unit is a tetrahedron of the two silicates that make up the dimer, and the surface reactive groups are present in the bridges and end chains of silica and aluminium. The area occupied by the dimer is 41.123Å$^2$ and is constant regardless of the Ca/(Si+Al) ratio [30-31]. Nonat proposed that the layered structure of C-S-H was a 60 × 30 × 5 nm elliptical cylinder [32]. Based on the above information and the results shown in **Fig. 4**, the density of surface sites presents in $Q^1$ and $Q^2$b can be calculated using the equations given below:

$$N_{s-Q^1} = \frac{S_{ellipse}}{S_{unit}} \times \frac{MCL}{2} \times \frac{1}{2} \times \frac{Q^1}{MCL} \times \frac{1}{S_{ellipse}} \times 2N_{lamella} \quad (1)$$

$$N_{s-Q_b^2} = \frac{S_{ellipse}}{S_{unit}} \times \frac{MCL}{2} \times \frac{1}{2} \times \frac{2 \times Q_b^2}{MCL} \times \frac{1}{S_{ellipse}} \times 2N_{lamella} \quad (2)$$

where $N_{s\text{-}Q}{}^{1}$ and $N_{s\text{-}Q}{}^{2}{}_{b}$ are the surface site density (sites/nm$^2$), $S_{ellipse}$ is the area of the ellipse (5654 nm$^2$), $S_{unit}$ is the area of the unit cell (0.41123 nm$^2$), *MCL* is the mean chain length of the silica chain, and $N_{lamella}$ is the number of staking layers. The estimated total surface site densities of C-S-H and C-A-S-H as a function of the Ca/(Si+Al) ratio is shown in **Fig. 5.** The site density increased with increasing Ca/(Si+Al) ratio due to the increase in the number of stacking layers. The quantified total surface site densities of C-S-H and C-A-S-H were 4.3–6.3 and 3.5–5.2 sites/nm$^2$, respectively. These values are not significantly different from those reported in the literature [13, 30-31, 33-35]; a value of 4.8 sites/nm$^2$ has been reported for C-S-H in many studies [30-31, 33].

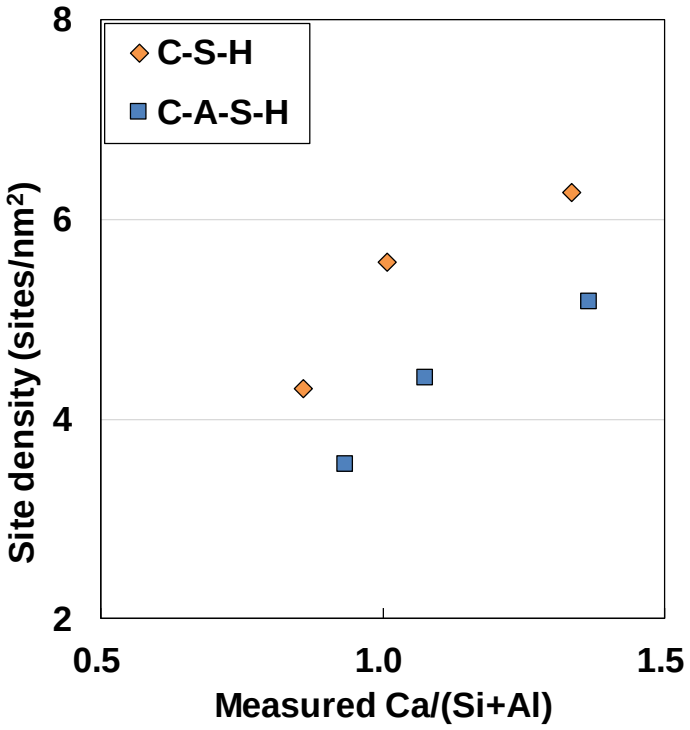


**Fig. 5.** Estimated total surface site density of C-S-H and C-A-S-H

### 3.2 Electrostatic interaction between C-A-S-H and hydroxyl, calcium, and chloride ions

The total sites determined in section 3.1 were divided further into strong and weak sites, where the weak sites were easy to dissociate, while the strong sites were difficult to dissociate. Charukov et al. performed a simulation based on the different degrees of dissociation in $Q^1$ and $Q^2b$, each of which exists at a ratio of 1:1 [33]. A similar approach was adopted in this study to estimate the density of weak and strong sites. In the silicate chain, $Q^2b$ exists only on the flat surface and is distributed to sites with different dissociation ratios of 1:1. However, $Q^1$ exists on both flat surface and edge, and the surface area ratio between the end surface and the layer surface can be calculated based on the layered structure proposed by Haas et al. [30]. The $Q^1$ sites on the flat surface can form a hydrogen bond and are considered to be strong sites, whereas the sites at the edge surface are less affected by hydrogen bonds and considered as weak sites. The strong and weak surface site densities of C-S-H and C-A-S-H are presented in **Table 3**.

The strong and weak of ≡SiOH and ≡AlOH surface sites are dissociated in the alkaline solution as follows:

$$\equiv XOH \rightleftharpoons \equiv XO^- + H^+ \qquad K_{OH} = \frac{(\equiv XO^-)*(a_{H^+})}{(\equiv XOH)} exp\left(-\frac{\Delta z_i F \psi_i}{RT}\right) \quad (3)$$

*X: Si* or *Al*

where $K_{OH}$ is the intrinsic equilibrium constant for dissociation, *(≡XOH), (≡XO⁻)* are concentrations of the surface species of surface sites (mol/m$^2$), $a_{H+}$ is the activity of $H^+$ (mol/L), $\psi_i$ is the potential at the 0-, 1-, or 2-plane (V), $\Delta z_i$ is the charge distribution, $R$ is the universal gas constant equal to 8.31451 J/(mol·K), and $T$ is the absolute temperature (K).

In the titration experiment, the pH of the solution containing C-S-H/C-A-S-H was lower than the initial blank pH because of the $H^+$ dissociation. The amount of dissociated $H^+$ can be calculated as follows [36]:

$$Excess/deficit\left[H^+\right] = \frac{(\left[H^+\right]_{initial} - \left[H^+\right]_{fin}) * (V_{initial} + V_{NaOH.add})}{(V_{initial} + V_{NaOH.add}) * A * SSA} \quad (4)$$

where $[H^+]_{initial}$ is the $H^+$ concentration in the blank solution (mol/L), $[H^+]_{fin}$ is the $H^+$ concentration in the solution containing sample (mol/L), $V_{initial}$ is the initial volume (mL), $V_{NaOH.add}$ is the amount of added NaOH (mL), *SSA* is the specific surface area ($m^2$/g), and *A* is the solid to liquid ratio (g/L).

The titration experimental results from Eq. (4) were fitted to the surface complexation modelling results to estimate the $K_{OH}$ of both strong and weak sites. It was assumed that a water molecule was attached to the inner and outer Stern layers of the triple-layer surface complexation model for the interaction of C-S-H/C-A-S-H in NaOH solution (**Fig. 1.**). An example of fitting results for C-S-H with a Ca/Si ratio of 1.5 is shown in **Fig. 6**. A similar fitting was performed for other C-S-H and C-A-S-H samples in NaOH solution. The estimated equilibrium constant for the dissociation of surface sites as a function of Ca/Si is shown in **Fig. 7** and presented in **Table 3**. The determined $pK_{OH}$ for weak and strong sites were 6.6 and 13.0, respectively, irrespective of Ca/Si or aluminium incorporation into the C-S-H. The results indicated that the surface of C-S-H/C-A-S-H was affected by the presence and ionisation of weak sites in NaOH solution, and not by the strong sites. The estimated equilibrium constants are comparable to the results reported in the literature; Pointeau et al. reported 7.6 for both strong and weak ≡SiOH sites [34], Hass and Nonat reported 7.7 for ≡SiOH [30], Elakneswaran et al reported 12.7 for ≡SiOH [8], Viallis-Terrisse et al. reported 12.3 [31] and Pointeau et al. reported 12.0 for ≡SiOH sites [13].

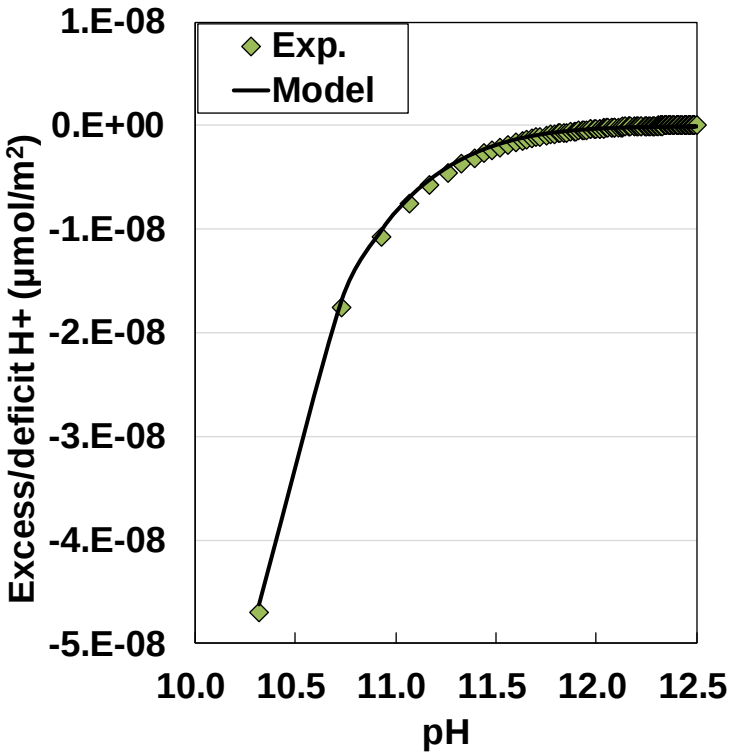


293

294 **Fig. 6.** Fitting of titration experimental data with modelling results for CSH:1.5

295

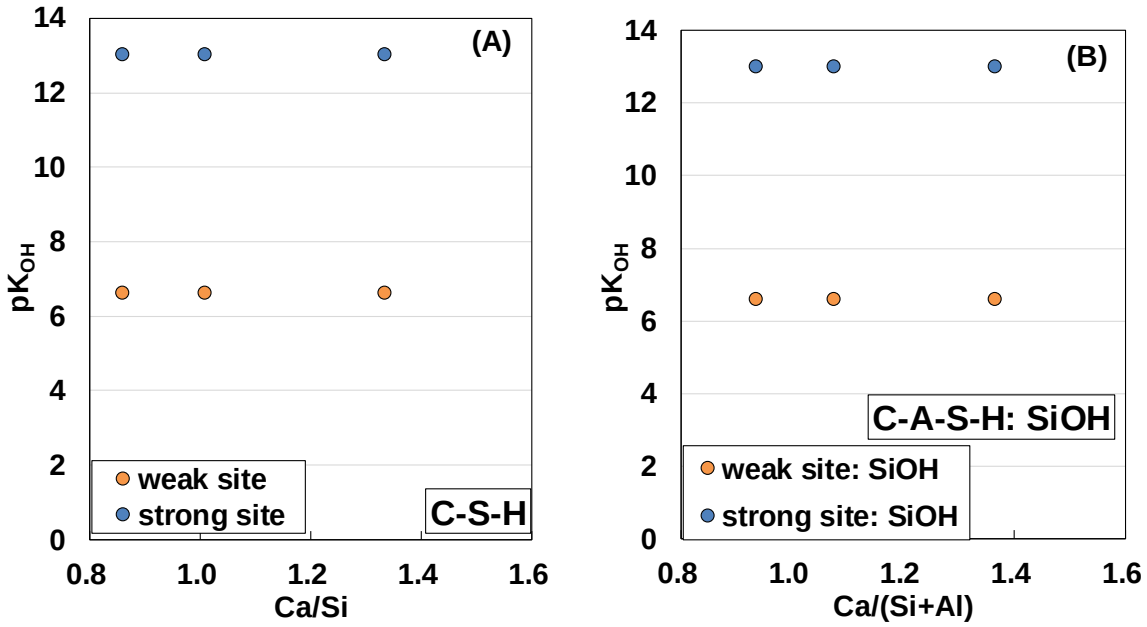


296

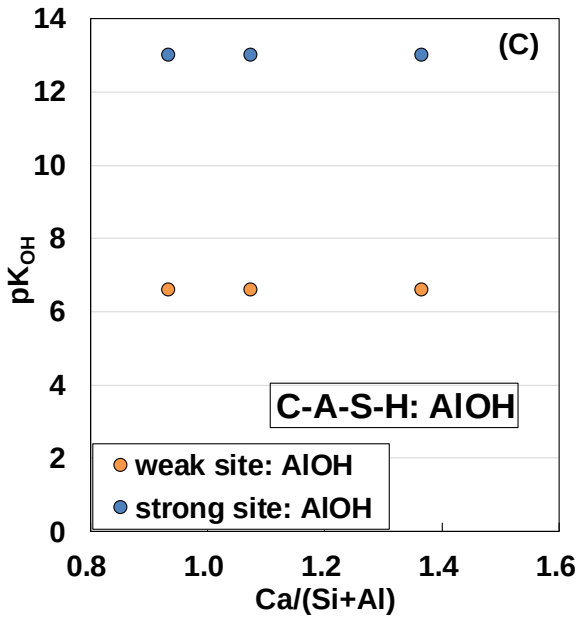


297

298 **Fig. 7.** Determined dissociation equilibrium constant for strong and weak sites: (A) ≡SiOH sites in

299 C-S-H; (B) ≡SiOH sites in C-A-S-H; (C) ≡AlOH sites in C-A-S-H.

300

301 To understand the interaction of $Ca^{2+}$ on the surface of C-S-H/C-A-S-H, zeta potential experiments

302 were conducted, and the results were fitted to surface complexation modelling results to develop a

303 model for $Ca^{2+}$ adsorption. The model considers the presence of $CaOH^{+}$ ions in the pH solution and

304 its adsorption on C-S-H/C-A-S-H. The adsorption of $Ca^{2+}$ and $CaOH^{+}$ on strong and weak ≡SiOH

305 and ≡AlOH surface sites was considered as the following inner-sphere surface complexation

306 reaction:

307

308 $$\equiv XOH + Ca^{2+} \rightleftharpoons \equiv XOCa^{+} + H^{+} \qquad K_{Ca} = \frac{(\equiv XOCa^{+})*(a_{H^{+}})}{(\equiv XOH)*(a_{Ca^{2+}})} exp\left(-\frac{\Delta z_i F \psi_i}{RT}\right)$$

309 (5)

310

311 $$\equiv XOH + Ca^{2+} + OH^{-} \rightleftharpoons \equiv XOCaOH + H^{+} \quad K_{CaOH} = \frac{(\equiv XOCaOH)*(a_{H^{+}})}{(\equiv XOH)*(a_{Ca^{2+}})*(a_{OH^{-}})} exp\left(-\frac{\Delta z_i F \psi_i}{RT}\right)$$

312 (6)

313 *X: Si* or *Al*

where $K_{Ca,}$ and $K_{CaOH}$ are the intrinsic equilibrium constants for calcium adsorption, $(\equiv XOCa^{+})$ and $(\equiv XCaOH)$ are the concentrations of the surface species of surface sites (mol/m$^2$), and $a_{Ca2+}$ is the activity of $Ca^{2+}$ (mol/L).

The experimental data for the C-S-H/C-A-S-H in $Ca(OH)_2$ solution were fitted to the modelling results to estimate $K_{Ca,}$and $K_{CaOH}$. An example of such fitting is shown in **Fig. 8**. Furthermore, the change in the determined equilibrium constant with Ca/Si is shown in **Fig. 9** and presented in **Table 3**. As observed for the dissociation of sites in the NaOH solution (**Fig. 7**), the weak sites significantly influence the adsorption of calcium ions. Moreover, the equilibrium constant of ≡AlOH is nearly equal to that of ≡SiOH.

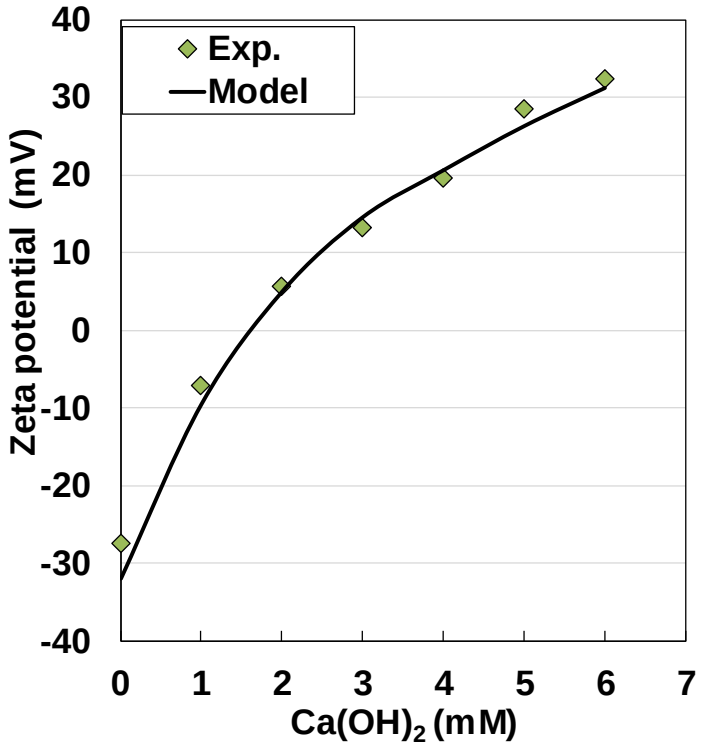


**Fig. 8.** Fitting of zeta potential experimental data with modelling results for CSH:1.5

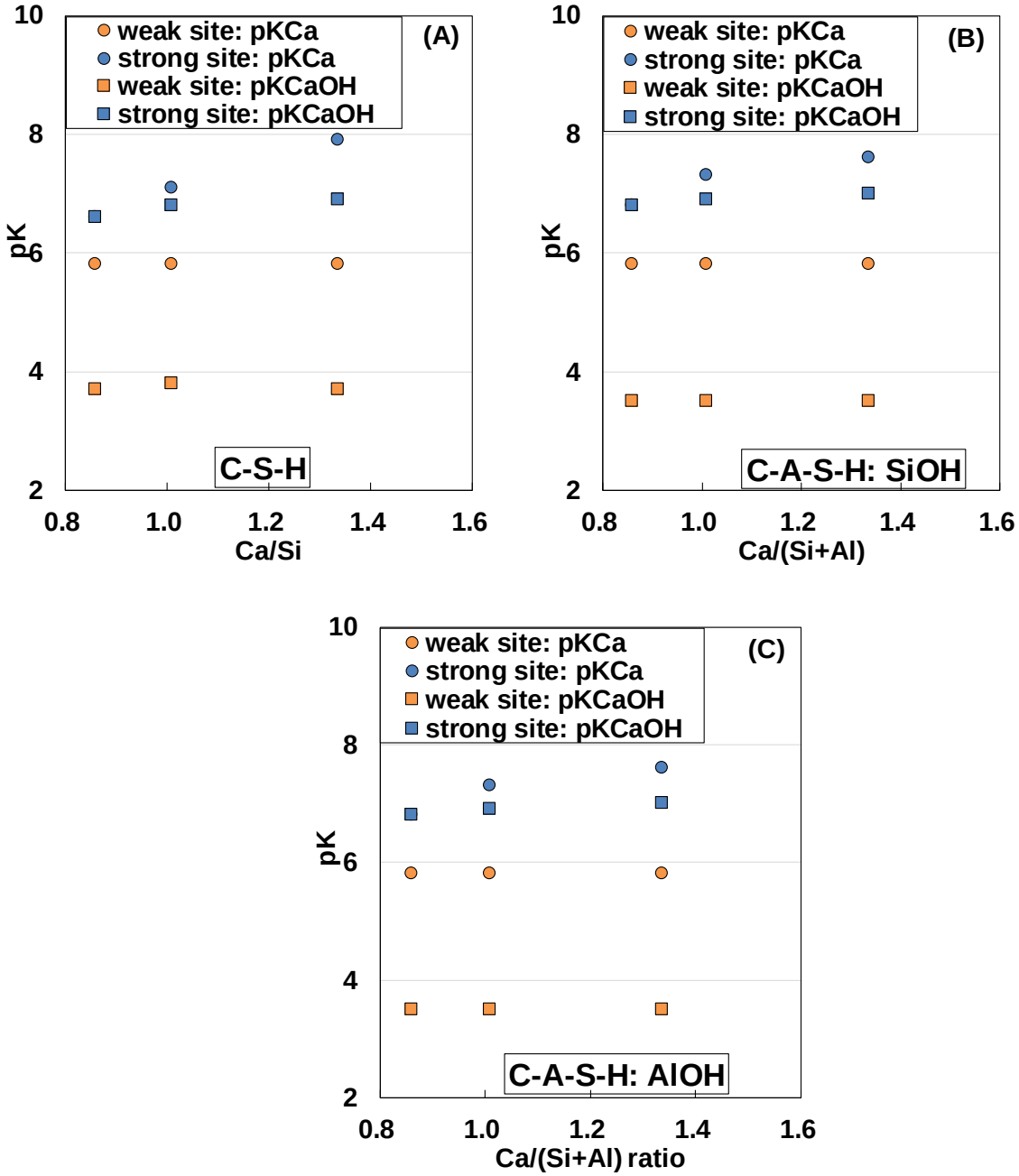


**Fig. 9.** Determined equilibrium constant of calcium absorption for strong and weak, (A) ≡SiOH sites in C-S-H; (B) ≡SiOH sites in C-A-S-H; (C) ≡AlOH sites in C-A-S-H. Note: pKCa and pKCaOH for strong site of CSH-0.8 and CASH-0.8 are identical values and overlap in the figure.

It has been reported that the associated divalent cation shows higher chloride binding compared with monovalent ions [14]. The positive surface of C-S-H/C-A-S-H strong and weak sites in the presence of calcium can adsorb chloride ions via the following surface complexation reaction:

$$\equiv XOH + Ca^{2+} + Cl^{-} \rightleftharpoons \equiv XOCaCl + H^{+} \qquad K_{CaCl} = \frac{(\equiv XOCaCl)*(a_{H^+})}{(\equiv XOH)*(a_{Ca^{2+}})(a_{Cl^-})} exp\left(-\frac{\Delta z_i F \psi_i}{RT}\right) \quad (7)$$

*X: Si* or *Al*

where $K_{CaCl}$ is the intrinsic equilibrium constant for chloride adsorption, *(≡XOCaCl)* is the concentration of the surface species of surface sites (mol/m$^2$), and $a_{Cl-}$ is the activity of $Cl^-$ (mol/L).

A similar approach was adopted for calcium used in here to estimate the equilibrium constant for chloride adsorption in the presence of calcium. The zeta potential results of C-S-H/C-A-S-H in $CaCl_2$ solution were fitted to the modelling results (an example is shown in **Fig. 10**). The estimated equilibrium constants for both C-S-H and C-A-S-H, as a function of Ca/Si, are shown in **Fig. 11** and presented in **Table 3**. Again, the weak sites control the chloride adsorption on C-S-H/C-A-S-H. Moreover, the equilibrium constant of the ≡AlOH group is smaller than that of ≡SiOH, indicating a higher chloride interaction towards ≡AlOH than that in ≡SiOH sites.

A summary of the determined surface site densities of C-S-H and C-A-S-H and their equilibrium constants is presented in **Table 3.** The fitted equilibrium constants for calcium and chloride adsorption on weak sites are constant regardless of the site density or Ca/Si. However, the equilibrium constant for strong sites increases with the site density or Ca/Si, which would affect the quantity of adsorbed ions.

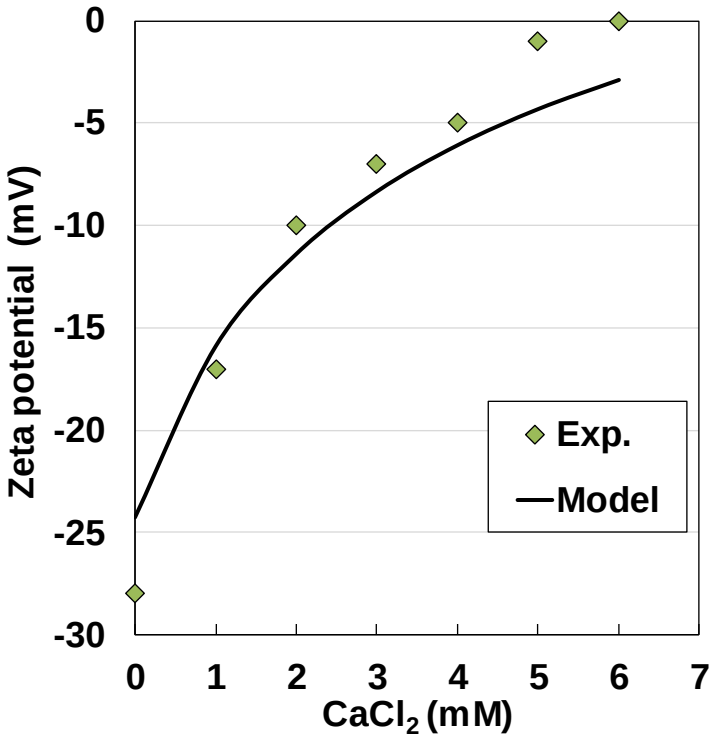


360

361 **Fig. 10.** Fitting of zeta potential experimental data with modelling results for CSH:1.5

362

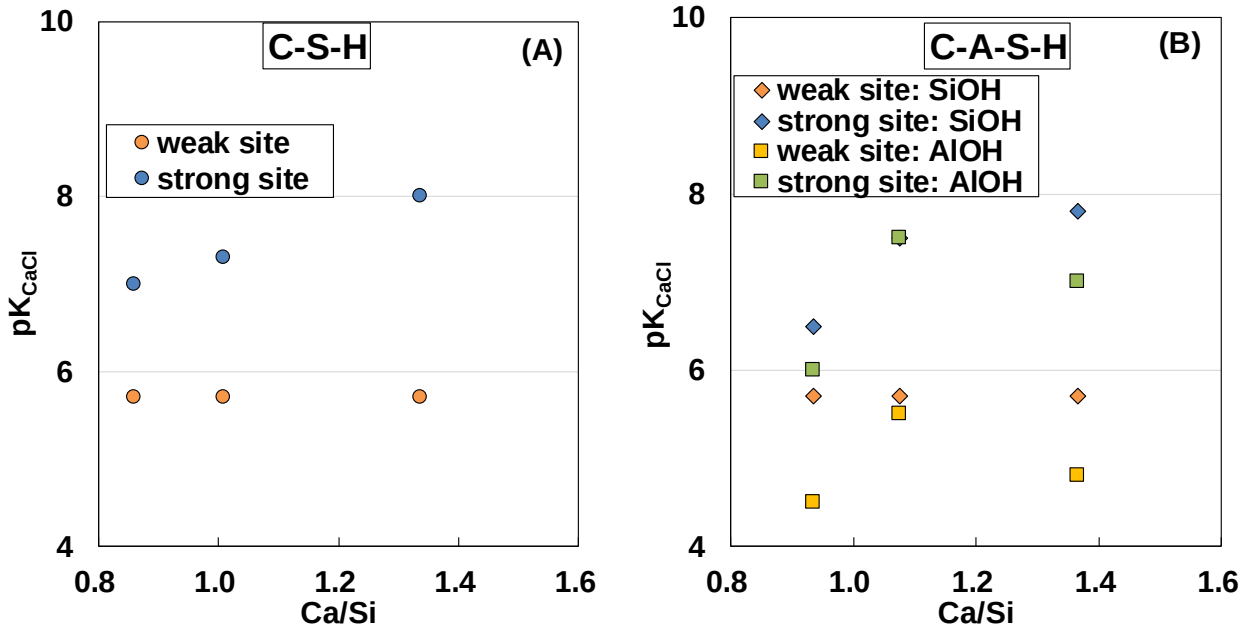


363

364 **Fig. 11.** Determined equilibrium constant of chloride adsorption for strong and weak, (A) ≡SiOH

365 sites in C-S-H; (B) ≡SiOH and ≡AlOH sites in C-A-S-H.

366

367

**Table 3:** Estimated surface complexation modelling parameters for C-S-H/C-A-S-H

| | | | Site density (sites/nm$^2$) | $pK_{OH}$ | $pK_{Ca}$ | $pK_{CaOH}$ | $pK_{CaCl}$ |
|---|---|---|---|---|---|---|---|
| **CSH-0.8** | **SiOH** | weak site | 1.54 | 6.6 | 5.8 | 3.7 | 5.7 |
| | | strong site | 2.76 | 13.0 | 6.6 | 6.6 | 7.0 |
| **CSH-1.0** | **SiOH** | weak site | 1.44 | 6.6 | 5.8 | 3.8 | 5.7 |
| | | strong site | 4.12 | 13.0 | 7.1 | 6.8 | 7.3 |
| **CSH-1.5** | **SiOH** | weak site | 1.13 | 6.6 | 5.8 | 3.7 | 5.7 |
| | | strong site | 5.14 | 13.0 | 7.9 | 6.9 | 8.0 |
| **CASH-0.8** | **SiOH** | weak site | 1.22 | 6.6 | 5.8 | 3.5 | 5.7 |
| | | strong site | 2.02 | 13.0 | 6.8 | 6.8 | 6.5 |
| | **AlOH** | weak site | 0.15 | 6.6 | 5.8 | 3.5 | 4.5 |
| | | strong site | 0.15 | 13.0 | 6.8 | 6.8 | 6.0 |
| **CASH-1.0** | **SiOH** | weak site | 1.07 | 6.6 | 5.8 | 3.5 | 5.7 |
| | | strong site | 2.89 | 13.0 | 7.3 | 6.9 | 7.5 |
| | **AlOH** | weak site | 0.22 | 6.6 | 5.8 | 3.5 | 5.5 |
| | | strong site | 0.22 | 13.0 | 7.3 | 6.9 | 7.5 |
| **CASH-1.5** | **SiOH** | weak site | 1.06 | 6.6 | 5.8 | 3.5 | 5.7 |
| | | strong site | 3.73 | 13.0 | 7.6 | 7.0 | 7.8 |
| | **AlOH** | weak site | 0.16 | 6.6 | 5.8 | 3.5 | 4.8 |
| | | strong site | 0.22 | 13.0 | 7.6 | 7.0 | 7.0 |

### 3.3 Prediction of calcium and chloride adsorption on C-A-S-H

The estimated surface complexation modelling parameters (**Table 3**) were used to predict the adsorption of calcium and chloride. The predicted calcium adsorption on C-S-H and C-A-S-H was compared with experimental data for different Ca/Si ratios in **Figs**. **12** and **13**, respectively. The

model successfully predicted calcium adsorption as a function of calcium concentration. As can be seen from the model prediction, both $Ca^{2+}$ and $CaOH^{+}$ adsorb on the surface sites, but the adsorption of $CaOH^{+}$ contributes at a high concentration of calcium. Therefore, both surface complexation reactions (Eqs. (5) and (6)) are necessary to understand calcium adsorption on C-S-H and C-A-S-H. The Ca/Si or Ca/(Si+Al) ratios significantly affect calcium adsorption; the adsorption decreases with an increase in the ratio (**Fig**. **12 (D)** and **Fig. 13 (D)**). This is due to the equilibrium pH and calcium concentration, which rise as the Ca/Si or Ca/(Si+Al) ratio increases [37]. Both experimental and modelling results indicate that aluminium incorporation in C-A-S-H does not influence the total calcium adsorption. The substitution of silica by aluminium decreases the total surface sites in C-A-S-H (**Fig. 5**), but a fraction of available silica sites changes to ≡AlOH sites. Therefore, both ≡SiOH and ≡AlOH sites contribute to calcium adsorption in C-A-S-H and show an equal amount of adsorption as in C-S-H.

The surface complexation reactions given in Eqs. (3), (5), (6) and (7) were used to predict chloride adsorption on C-S-H and C-A-S-H in $CaCl_2$ solution. A high concentration of $CaCl_2$ solution was selected to enhance chloride adsorption on C-S-H and C-A-S-H, as reported in ref. [12] where 20–70% of chloride adsorption was observed when cement paste was exposed to $CaCl_2$ solutions. Both the strong and weak of the ≡SiOH and ≡AlOH sites compete for chloride adsorption via the surface complexation reaction given in Eq. (7). However, the surface site density and equilibrium constants presented in **Table 3** control the amount of adsorption. A comparison between the predicted and measured chloride adsorption on C-S-H and C-A-S-H is shown in **Figs. 14** and **15**, respectively. A very good agreement between the predicted results and experimental data indicates the validity of the model and estimated parameters. Both experimental data and modelling results show that aluminium incorporation in C-S-H reduces chloride adsorption irrespective of the Ca/Si ratio.

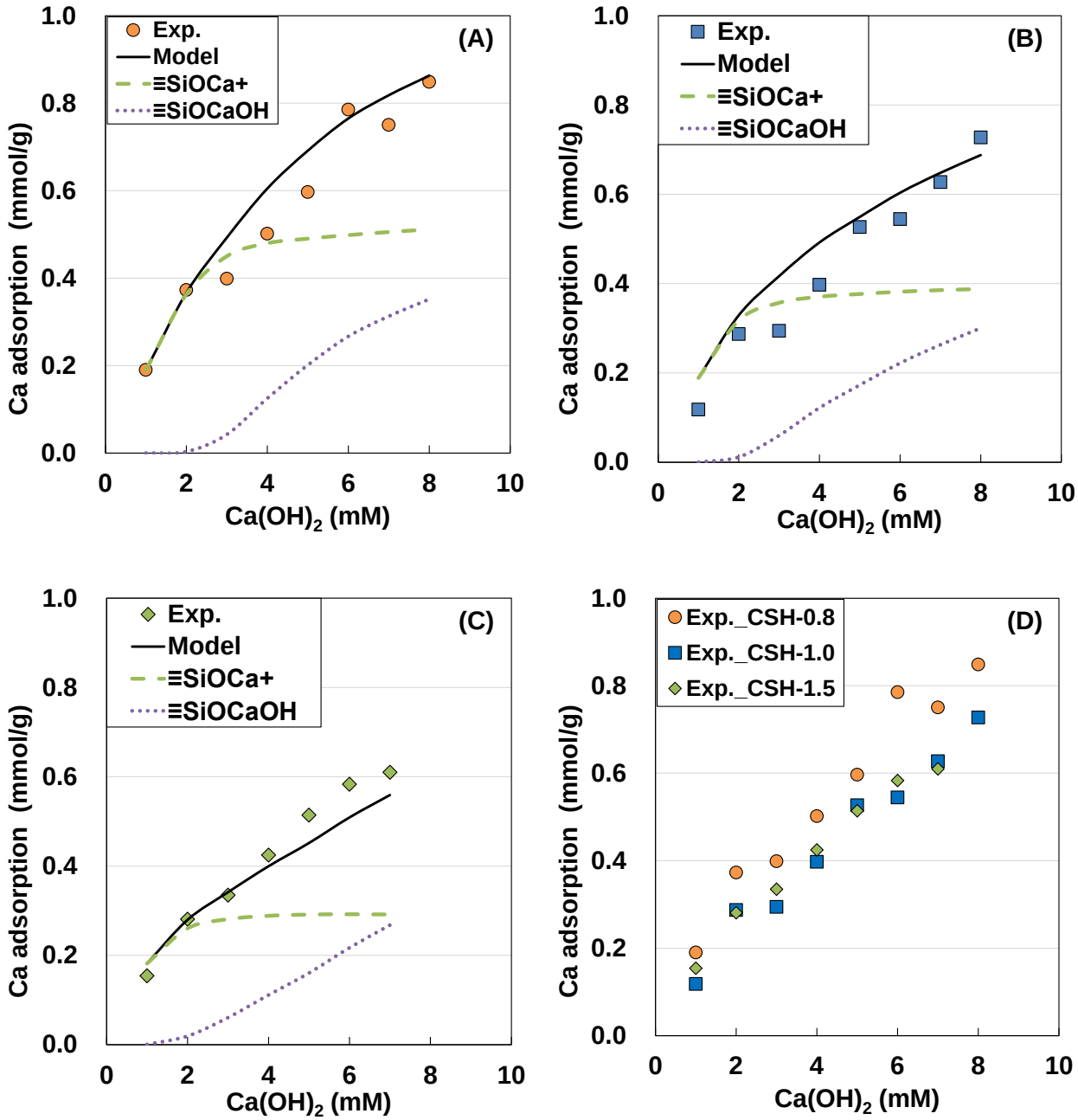


**Fig. 12.** Comparison of the predicted and measured calcium adsorption on C-S-H with (A) Ca/Si of 0.8; (B) Ca/Si of 1.0; (C) Ca/Si of 1.5. (D) Comparison of the measured calcium adsorption on C-S-H with different Ca/Si ratios.

403

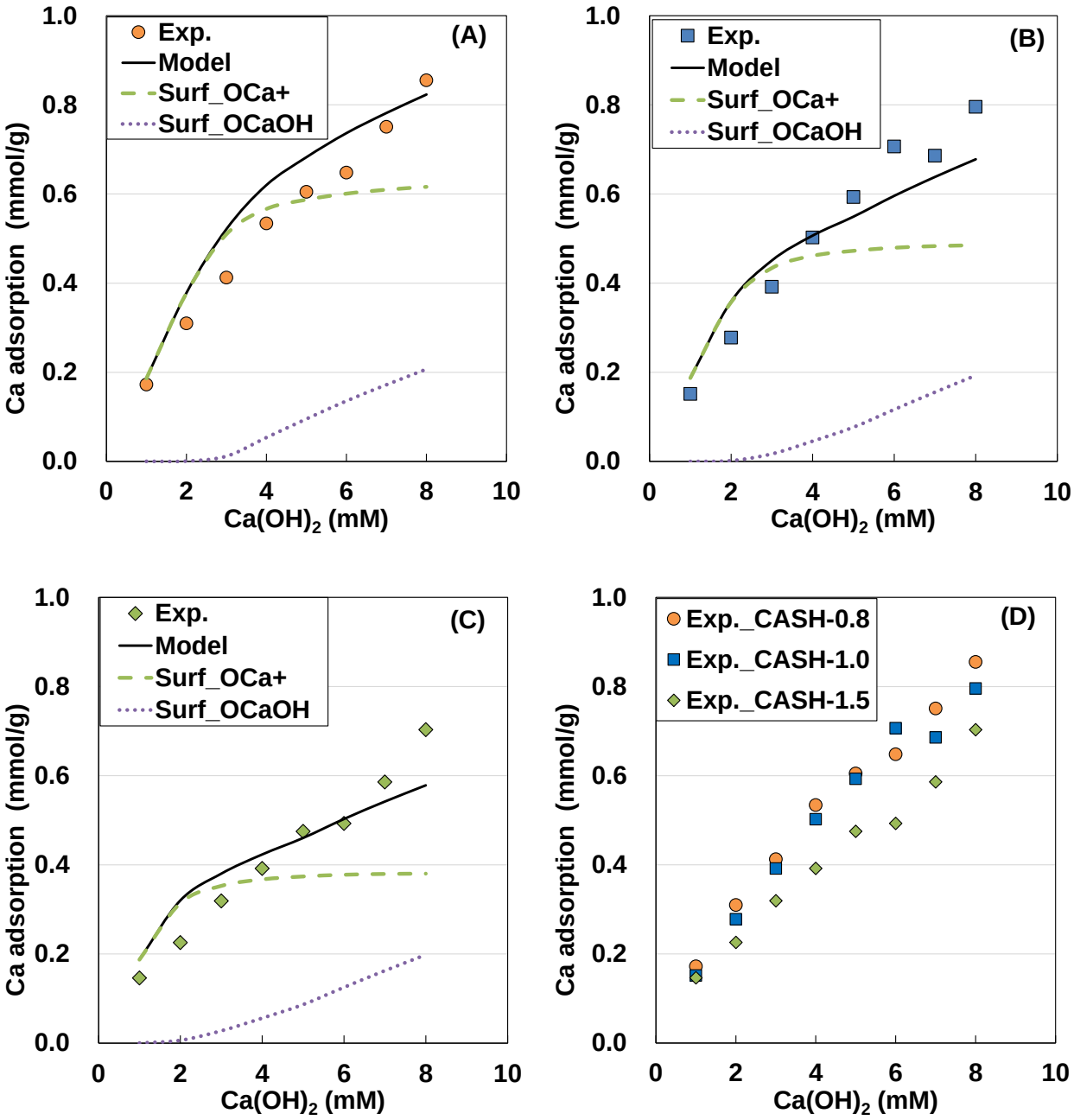


404

405 **Fig. 13.** Comparison of the predicted and measured calcium adsorption on C-A-S-H with (A)

406 Ca/(Si+Al) of 0.8; (B) Ca/(Si+Al) of 1.0; (C) Ca/(Si+Al) of 1.5. (D) Comparison of the measured

407 calcium adsorption on C-A-S-H with different Ca/(Si+Al) ratios.

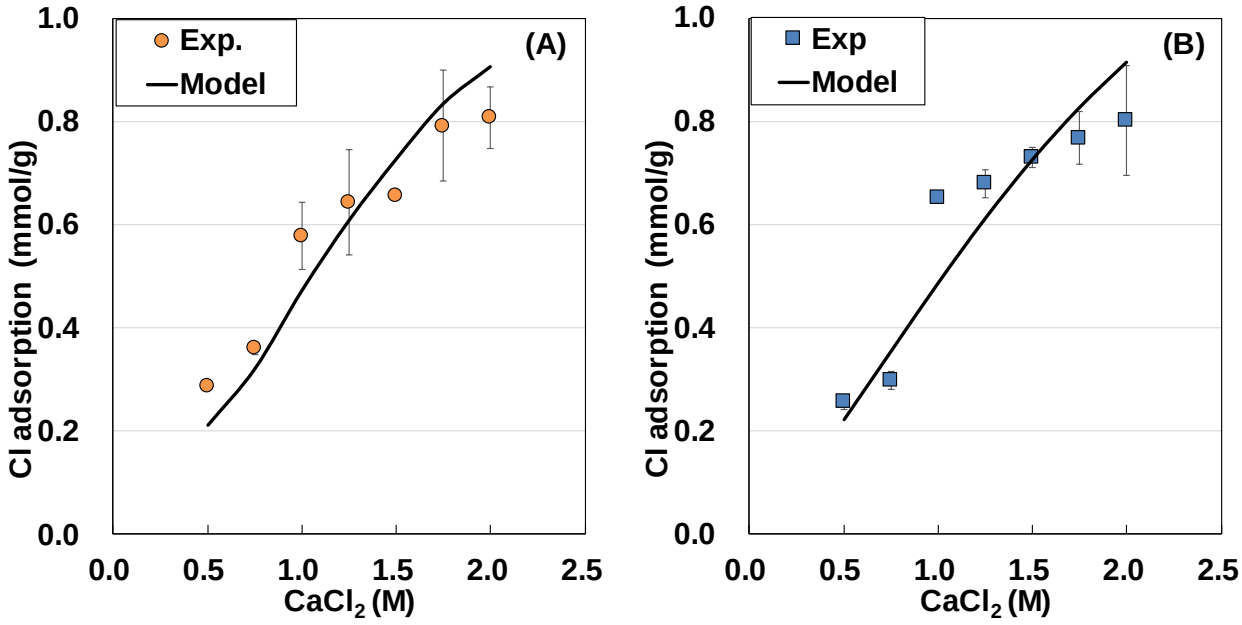


408

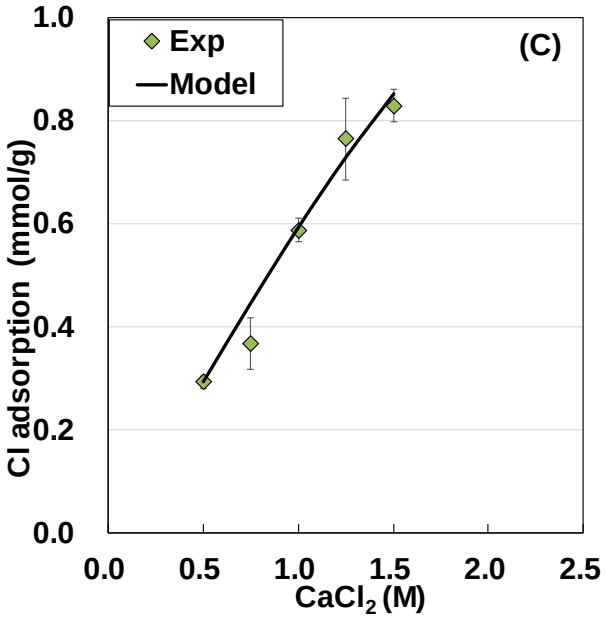


409

410 **Fig. 14.** Comparison of the predicted and measured chloride adsorption on C-S-H with (A) Ca/Si of

411 0.8; (B) Ca/Si of 1.0; (C) Ca/Si of 1.5.

412

413

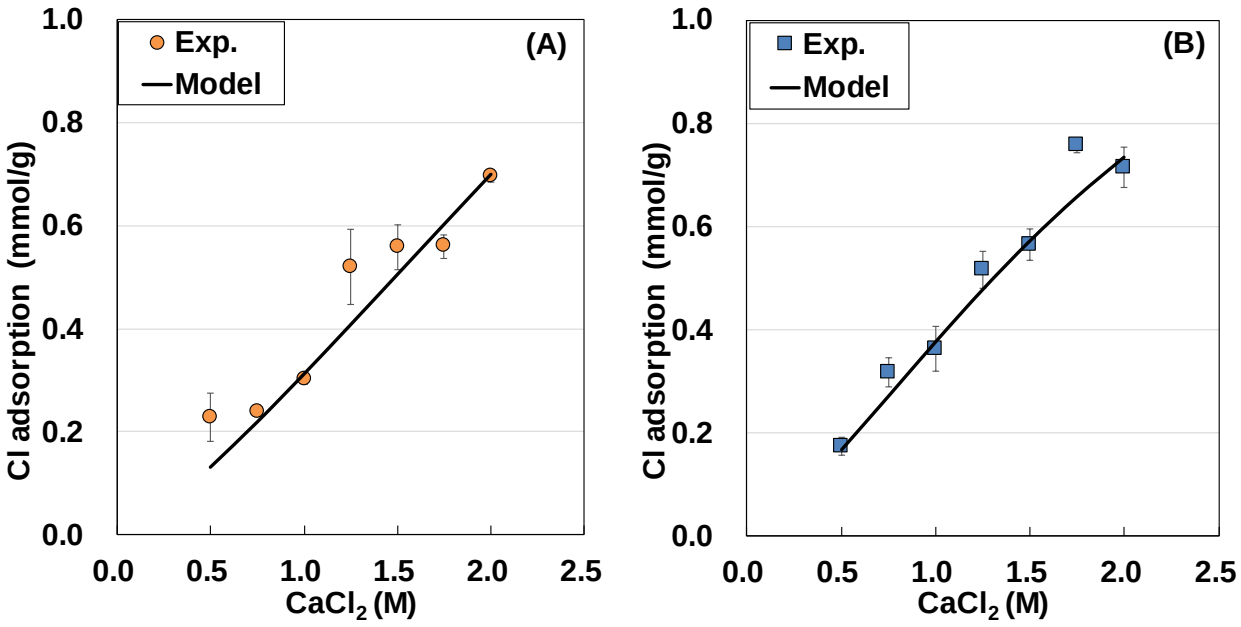


414

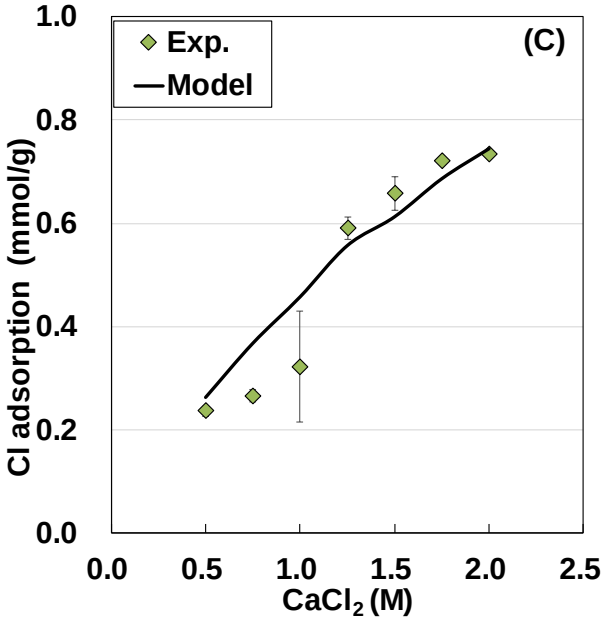


415

416 **Fig. 15.** Comparison of the predicted and measured chloride adsorption on C-A-S-H with (A)
417 Ca/(Si+Al) of 0.8; (B) Ca/(Si+Al) of 1.0; (C) Ca/(Si+Al) of 1.5.

418

419 **4. Conclusions**

420 The electrostatic interaction of calcium and chloride ions on C-S-H and C-A-S-H was evaluated by
421 experiments and a triple-layer surface complexation model. C-S-H and C-A-S-H were characterised
422 to determine the surface functional groups and their densities: C-S-H possesses strong and weak
423 ≡SiOH sites, whereas C-A-S-H has strong and weak ≡SiOH and ≡AlOH sites. The chemical

composition of C-S-H/C-A-S-H affects the site density, which increases with the Ca/(Si+Al) ratio, but aluminium substitution decreases the site density at each Ca/(Si+Al) ratio. The CD-MUSIC triple-layer model built-in PHREEQC was used to understand the interaction of pH, calcium, and chloride ions with C-S-H and C-A-S-H. The equilibrium constants for the dissociation and adsorption of calcium and chloride were derived by fitting the experimental data to the modelling results. Moreover, the effect of the Ca/(Si+Al) ratio and aluminium incorporation on the equilibrium constant were evaluated. It was found that weak sites have high affinity for hydroxyl, calcium, and chloride ions. The validity of the determined site density and equilibrium constant values were tested against the batch adsorption experimental data. The modelling results agree well with the experimental data for both C-S-H and C-A-S-H, as a function of calcium or chloride concentration. Aluminium incorporation in C-S-H did not influence the calcium adsorption, but it reduced chloride adsorption in each Ca/Si ratio.

**Acknowledgments**

This study was financially supported by the Japan Society for the Promotion of Science (JSPS) Grants-in-Aid for Scientific Research (KAKENHI) Grant No. 18K0429708.

**References**

[1] V. M. Malhorta, Durability of concrete, Corrosion handbook, 2nd Ed., R. W. Revie, ed., Wiley, Hoboken, NJ. (2000).

[2] L. Tang, L-O. Nilsson, Chloride binding capacity and binding isotherms of OPC pastes and mortars, Cem. Concr. Res. 23 (1993) 247–253.

[3] Y. Elakneswaran, A. Iwasa, T. Nawa, T. Sato, K. Kurumisawa, Ion-cement hydrate interactions govern multi-ionic trans- port model for cementitious materials, Cement Concr. Res. 40 (2010) 1756–1765.

[4] V. Q. Tran, A. Soive, V. Baroghel-Bouny, Modelisation of chloride reactive transport in

concrete including thermodynamic equilibrium, kinetic control and surface complexation, Cement Concr. Res. 110 (2018) 70–85.

[5] J. J. Beaudoin, V. S. Ramachandran, and R. F. Feldman, “Interaction of chloride and C-S-H.” Cement Concr. Res. 20 (1990) 875–883.

[6] H. Hirao, K. Yamada, H. Takahashi, and H. Zibara, Chloride binding of cement estimated by binding isotherms of hydrates, J. Adv. Concr. Technol., 3 (2005) 77–84.

[7] Y. Cao, L. Guo, B. Chen, J. Wu, Thermodynamic modelling and experimental investigation on chloride binding in cement exposed to chloride and chloride-sulfate solution, Construct. Build. Mater. 246 (2020) 118398.

[8] Y. Elakneswaran, T. Nawa, K. Kurumisawa, Electrokinetic potential of hydrated cement in relation to adsorption of chlorides. Cement Concr. Res. 39 (2009) 340–344.

[9] H. W. Song and V. Saraswathy, Studies on the corrosion resistance of reinforced steel in concrete with ground granulated blast-furnace slag-an overview, J. Hazard. Mater. B, 138 (2006) 226–233.

[10] Y. Elakneswaran, T. Nawa, K. Kurumisawa, Influence of Surface Electrical Properties of C-S-H on Chloride Binding in Slag-Blended Cementitious Materials, J. Mater. Civ. Eng. 30 (2018) 04018064.

[11] K. Sasaki and T. Saeki, Chloride binding capacity of calcium silicate hydrate, Cem. Sci. Concr. Technol., 60 (2006) 322–327.

[12] C. Qiao, P. Suraneni, T. N. W. Ying, A. Choudhary, J. Weiss, Chloride binding of cement pastes with fly ash exposed to CaCl2 solutions at 5 and 23 °C, Cement Concr. Compos. 97 (2019) 43–53.

[13] I. Pointeau, P. Reiller, N. Mace, C. Landesman, N. Coreau, Measurement and modeling of the surface potential evolution of hydrated cement pastes as a function of degradation, Journal of Colloid and Interface Science, 300 (2006) 33–44.

[14] K. De Weerdt, A. Colombo, L. Coppola, H. Justnes, M. R. Geiker, Impact of the associated

476 cation on chloride binding of Portland cement paste, Cement Concr. Res. 68 (2015) 196–202
477 [15] G. Plusquellec and A. Nonat, Interactions between calcium silicate hydrate (CSH) and
478 calcium chloride, bromide and nitrate, Cement Concr. Res. 90 (2016) 89–96.
479 [16] Y. Zhou, D. Hou, J. Jiang, L. Liu, W. She, J. Yu, Experimental and molecular dynamics
480 studies on the transport and adsorption of chloride ions in the nano-pores of calcium silicate
481 phase: the influence of calcium to silicate ratios, Microporous and Mesoporous Materials
482 255(2018) 23–35.
483 [17] B. Lothenbach, K. Scrivener, R. D. Hooton, Supplementary cementitious materials, Cement
484 Concr. Res. 41 (2011) 1244–1256.
485 [18] I. G. Richardson, Model structures for C-(A)-S-H (I), Acta Cryst. B70 (2014). 903–923.
486 [19] I. G. Richardson, Tobermorite/jennite- and tobermorite/calcium hydroxide-based models for
487 the structure of C-S-H: applicability to hardened pastes of tricalcium silicate, β-dicalcium
488 silicate, Portland cement, and blends of Portland cement with blast-furnace slag, metakaolin,
489 or silica fume, Cement Concr. Res. 34 (2004) 1733–1777.
490 [20] X. Pardal, F. Brunet, T. Charpentier, I. Pochard, A. Nonat, $^{27}$Al and $^{29}$Si Solid-State NMR
491 Characterization of CalciumAluminosilicate-Hydrate, Inorg. Chem., 51 (2012) 1827–1836.
492 [21] E. L'Hôpital, Aluminium and alkali uptake in calcium silicate hydrate (C-S-H), PhD thesis,
493 ÉCOLE POLYTECHNIQUE FÉDÉRALE DE LAUSANNE (2014).
494 [22] E. L'Hôpital, B. Lothenbach, K. Scrivener, D. Kulik, Alkali uptake in calcium alumina
495 silicate hydrate (CASH), Cement Concr. Res. 85 (2016) 122–136.
496 [23] S. Y. Hong, F. P. Glasser, Alkali sorption by C-S-H and C-A-S-H and C-A-S-H gels PartII.
497 Role of alumina, Cement Concr. Res. 32 (2002) 1101–1111.
498 [24] D. Hou, T. Li, P. Wang, Molecular Dynamics Study on the Structure and Dynamics of NaCl
499 solution Transport in the Nanometer Channel of CASH Gel, ACS Sustainable Chem 6 (2018),
500 9498–9509.

[25] Parkhurst, D. L., and Appelo, C. A. J. “User’s guide to PHREEQC (Version 2)—A computer program for speciation, batch-reaction, one- dimensional transport and inverse geochemical calculations.” Water- Resources Investigations Rep. (1999). 99–4259, USGS, Denver.

[26] PHREEQC [Computer software]. United States Geological Survey, Reston, VA.

[27] T. Hiemstra, W. H. van Riemsdijk, A surface structural approach to ion adsorption: the charge distribution (CD) model, Journal of Colloid and Interface Science 179 (1996) 488–508.

[28] R. Rahnemaie, T. Hiemstra, W. H. van Riemsdijk, A new surface structural approach to ion adsorption: Tracing the location of electrolyte ions, Journal of colloid and interface science 293 (2006) 312–321.

[29] R. Myers, E. L’Hopital, J. L. Provis, B. Lothenbach, Effect of temperature and aluminium on calcium (alumino) silicate hydrate chemistry under equilibrium conditions, Cement Concr. Res. 68 (2015) 83–93.

[30] J. Haas and A. Nonat, From C–S–H to C–A–S–H: Experimental study and thermodynamic modelling, Cement Concr. Res. 68 (2015) 124–138.

[31] Viallis-Terrisse, A. Nonat, J. C. Petit, Zeta-potential study of calcium silicate hydrates interacting with alkaline cations, Journal of colloid and interface science 244 (2001) 58–65.

[32] A. Nonat, The structure and stoichiometry of CSH, Cement Concr. Res. 34 (2004) 1521–1528.

[33] S. V. Churakov, C. Labbez, L. Pegado, M. Sulpizi, Intrinsic Acidity of Surface Sites in Calcium Silicate Hydrates and Its Implication to Their Electrokinetic Properties, The journal of physical chemistry C, 118 (2014) 11752−11762.

[34] I. Pointeau, N. Marmier, F. Fromage, M. Fedoroff, E. Giffaut, Cs and Pb uptake by CSH phases of hydrated Cement. Material Research Society Symposium Proceedings 663 (2001) 105–113.

[35] M. Ochs, I. Pointeau, E. Giffaut, Caesium sorption by hydrated cement as a function of degradation state: Experiments and modelling, Waste Management 26 (2006) 725–732.

[36] C. Mayant, B. Grambow, A. Abdelouas, S. Ribet, S. Leclercq, Surface site density, silicic acid retention and transport properties of compacted magnetic powder, Phys. Chem. Earth, 33 (2008) 991–999.

[37] C. S. Walker, S. Sutou, C. Oda, M. Mihara, A. Honda, Calcium silicate hydrate (C-S-H) gel solubility data and a discrete solid phase model at 25 °C based on two binary non-ideal solid solutions, Cement Concr. Res. 79 (2016) 1–30.

# Appendix A

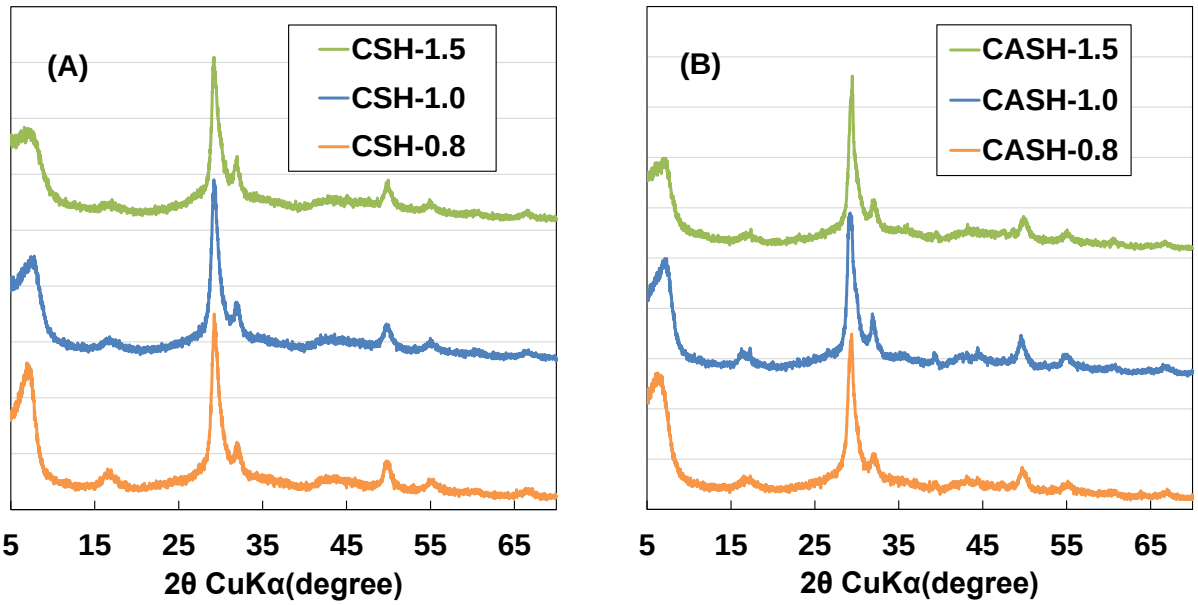


**Fig. A1.** XRD pattern of (A) C-S-H and (B) C-A-S-H

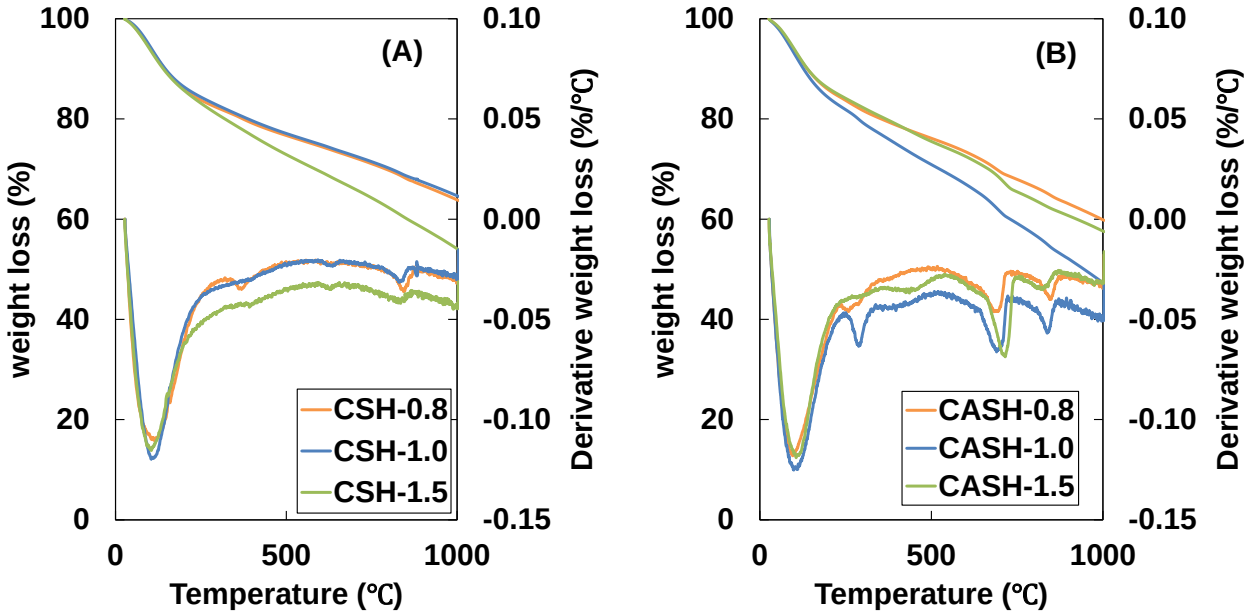


538

539 **Fig. A2.** TGA of (A) C-S-H and (B) C-A-S-H

540

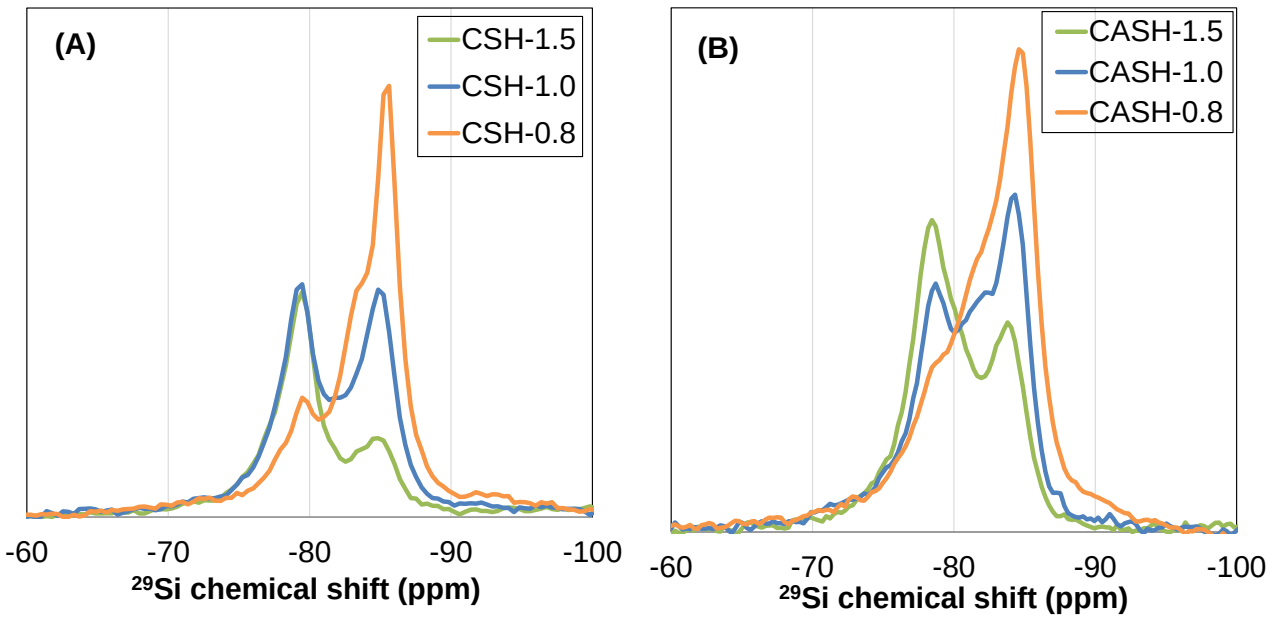


541

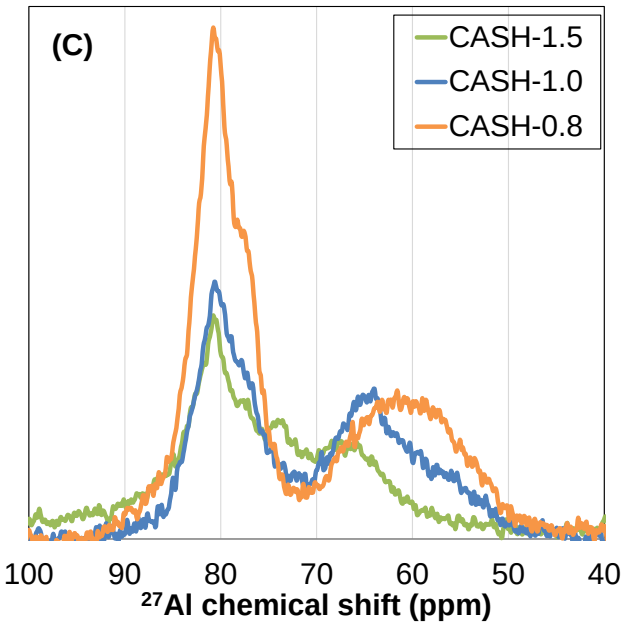


542

543 **Fig. A3.** (A) $^{29}$Si NMR of C-S-H; (B) $^{29}$Si NMR of C-A-S-H; and (C) $^{27}$Al NMR of C-A-S-H

544

**Declaration of interests**

☒ The authors declare that they have no known competing financial interests or personal relationships that could have appeared to influence the work reported in this paper.

☐The authors declare the following financial interests/personal relationships which may be considered as potential competing interests:

| |
|---|
| |